Supplementary Information

Injection- Seeded Optoplasmonic Amplifier in the Visible

Manas Ranjan Gartia, Sujin Seo, Junhwan Kim, Te-Wei Chang,
Gaurav Bahl, Meng Lu, Gang Logan Liu, and J. Gary Eden

This document contains the following supplementary information:

1. Optical and SEM images of the plasmonic substrate

    - Optical micrograph of wafer-scale plasmonic substrate

    - Cross-sectional SEM of a Si nanocone array

    - SEM of d = 2 μm polystyrene spheres

    - SEM of the microsphere on a plasmonic substrate

2. Optical System

3. Signal-to-Noise Ratio (SNR) for dye-conjugated microspheres illuminated at 632.8 nm

4. Optical images of dye-conjugated microspheres

5. Spectroscopic characterization of plasmonic substrate and dyes; Microsphere modes

    - Reflectance spectrum of plasmonic substrate

    - Absorption/ emission spectra of dyes (Cy-3, DyLight 650)

    - TE and TM WGMs in the 630 – 750 nm region (d = 10.1 μm)

6. Characterization of the laser spot size and detection system linearity

7. FEM simulation of the radial and azimuthal electric field amplitudes for d = 2 μm microspheres

8. FEM simulation of radial and polar modes for d = 2 μm microspheres

9. FDTD simulations of electric field spatial distributions and enhanced radiative rates for optoplasmonic amplifiers with d = 2 μm microspheres

10. Photoluminescence spectra of Ag-overcoated Si nanocone arrays

11. Impact of Ag nanolayer on the microresonator Q

12. Linear dependence of peak dye fluorescence intensity on dye concentration (100 nM – 1 μM)

13. Lifetime measurement for optoplasmonic system with Cy-3 dye

14. Photoluminescence spectra for an optoplasmonic structure when the dye lies at the interface between the polystyrene sphere and the plasmonic array, and not tethered to the microresonator

15. Raman spectrum and band assignment for Cy-5 dye

1. Optical and SEM images of the plasmonic substrate

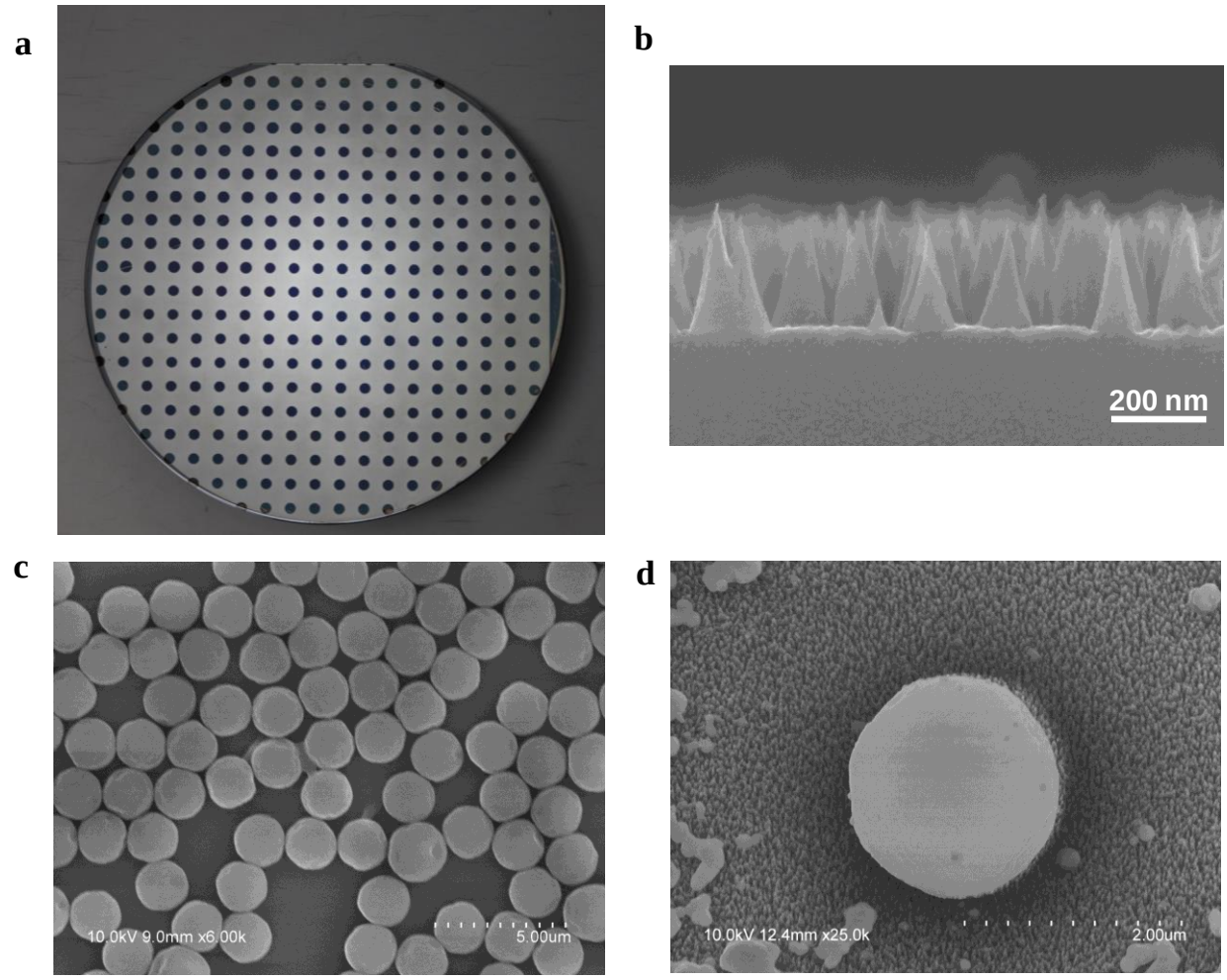

Figure S1: (a) Optical micrograph of Ag-overcoated Si nanocone arrays patterned onto a 4-inch (10 cm) diameter Si wafer. Regions of the wafer processed as an array appear as black circular spots whereas the unprocessed portions of the substrate are reflective. (b) Cross-sectional SEM of a portion of a Si nanocone array prior to deposition of the Ag overcoat. (c) SEM image of an

ensemble of d = 2 μm microspheres. (d) An SEM of a single, 2 μm diameter microsphere placed onto an Ag/Si nanocone array.

2. Optical System

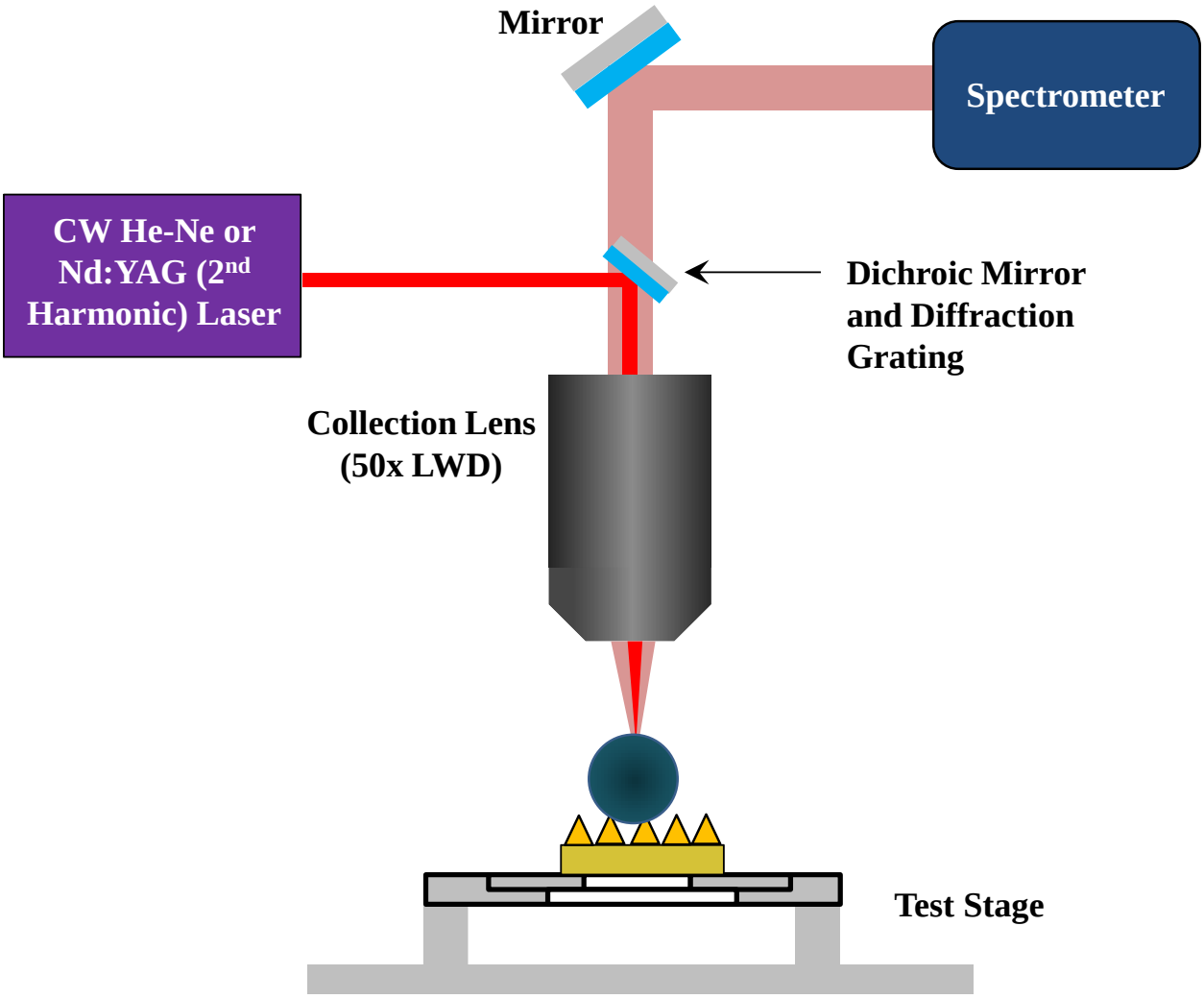

Figure S2: Schematic diagram of the optical arrangement employed throughout the experiments.

3. Signal-to-Noise Ratio (SNR) for dye-conjugated microspheres illuminated at 632.8 nm

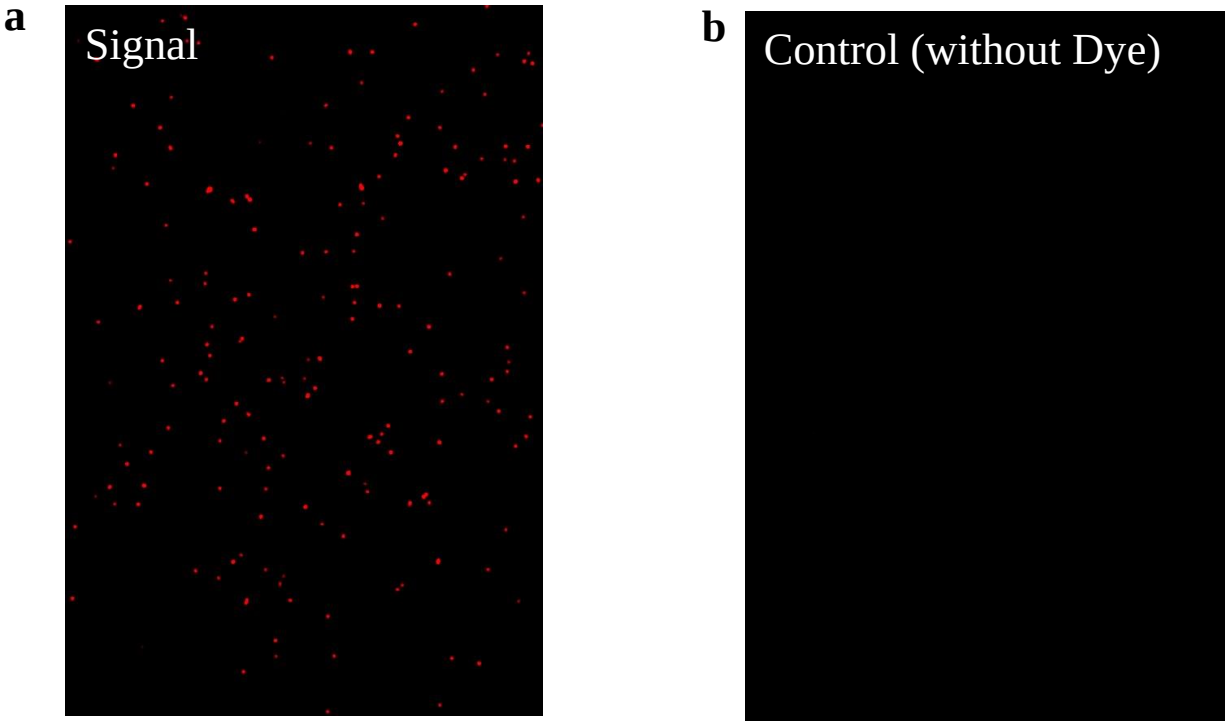

Figure S3: (a) Optical micrograph of d = 10.1 µm polystyrene spheres, coated with NeutrAvidin conjugated with a dye (DyLight 650) and irradiated at 632 nm with a Tecan laser scanner. A 690 nm filter rejected back-scattered pump laser radiation, and the detection system gain and excitation laser angle of incidence were 180 and 20°, respectively. Photoluminescence signal intensities from the spheres were in the range of 6 x 10^3 - 2 x 10^4 counts which correspond to signal-to-noise ratios (SNRs) between 120 and 400. (b) Optical image of a control sample, comprising microspheres without NA-DyLight 650 but having the sample areal density as that for (a). The spatial resolution for the image is also the same as that for (a).

4. Optical images of dye-conjugated microspheres

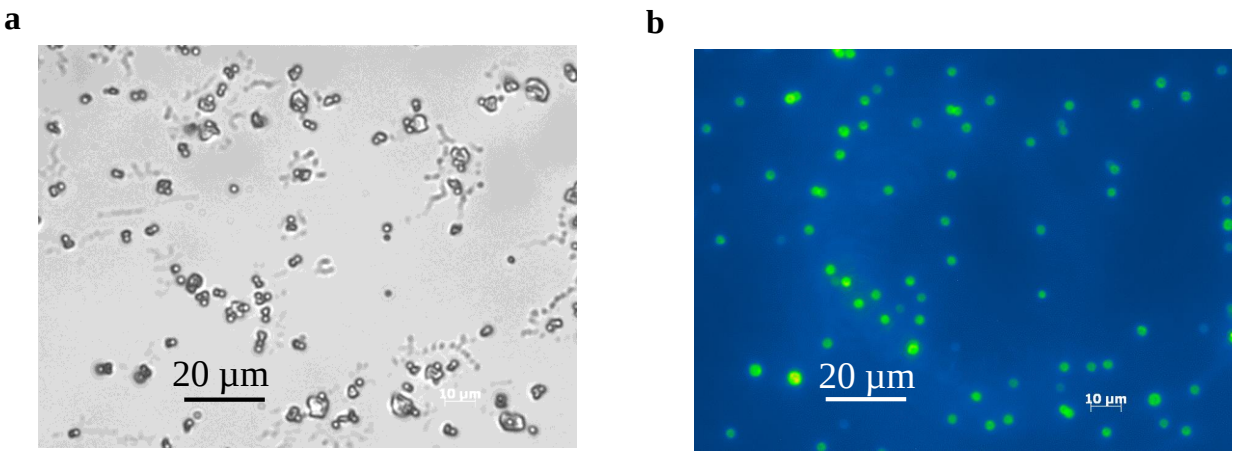

Figure S4: (a) Bright field image of 2 µm diameter spheres conjugated with NA-Dy, and imaged by a 50x objective. (b) Corresponding false color image of the fluorescence generated by the spheres when the dye is DyLight 650 and λ_p = 632.8 nm.

5. Spectroscopic characterization of plasmonic substrate and dyes; Microsphere modes

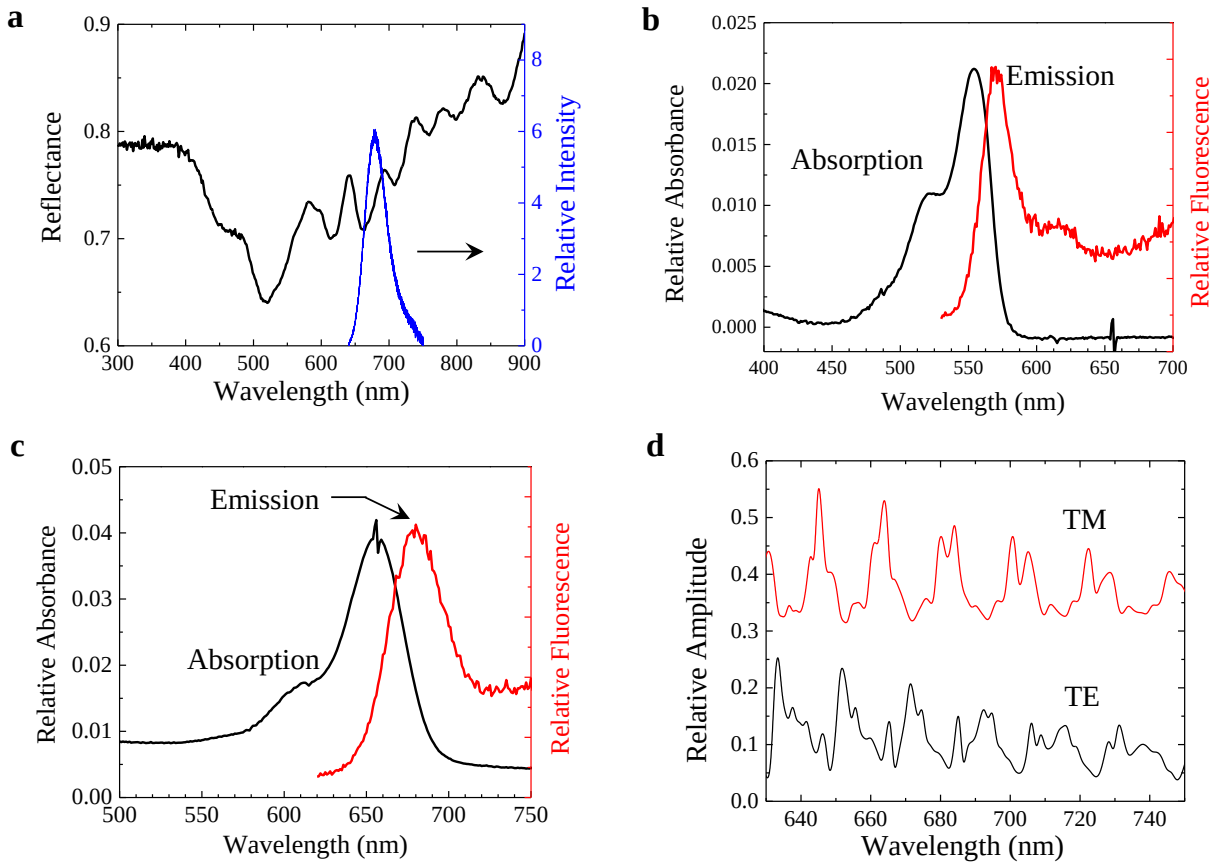

Figure S5: (a) Reflectance spectrum of the plasmonic surface (black curve). The undulatory structure confirms the ability of the Ag/Si substrate to support multiple plasmonic modes. For convenience, the photoluminescence spectrum observed when the red dye DyLight 650 is excited at 632.8 nm is also shown (blue profile). (b) Absorption (black trace) and fluorescence (red) spectra for the green dye Cy-3 attached to Neutravidin (biotin-avidin). (c) Spectra similar to those of (b) but associated with the red dye DyLight 650. (d) TE (black curve) and TM (red) WGM spectra in the 630 – 750 nm interval, calculated for 10.1 µm dia. polystyrene spheres with FDTD software.

6. Characterization of the laser spot size and detection system linearity

In order to determine the beam width of the excitation source, a scanning knife-edge method was adopted[1, 2]. The relative intensity of the 521 cm^{-1} Raman signal, emanating from the focal region at the surface of a Si wafer, was monitored as the laser was scanned along the coordinate orthogonal to the wafer edge (defined by cleaving). If the wafer edge is located $x = x_0$, then the strength of the Raman signal will vary with x as: $I(x) = \frac{I_{max}}{2}\left[1 + erf\left(\frac{\sqrt{2}(x_0 - x)}{w_0}\right)\right]$, where $erf(x)$ is the error function. Fitting this expression to the experimental results (shown below), the beam spot size w_0 was found to be 1.1 μm.

a

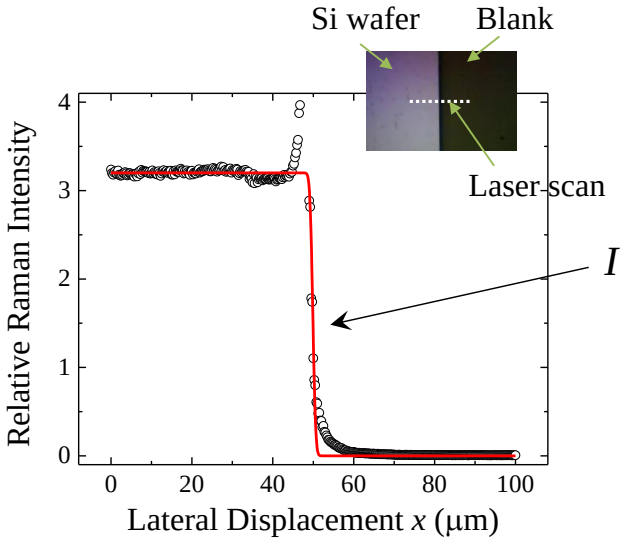

$$I(x) = \frac{I_{max}}{2}\left[1 + erf\left(\frac{\sqrt{2}(x_0 - x)}{w_0}\right)\right]$$

b

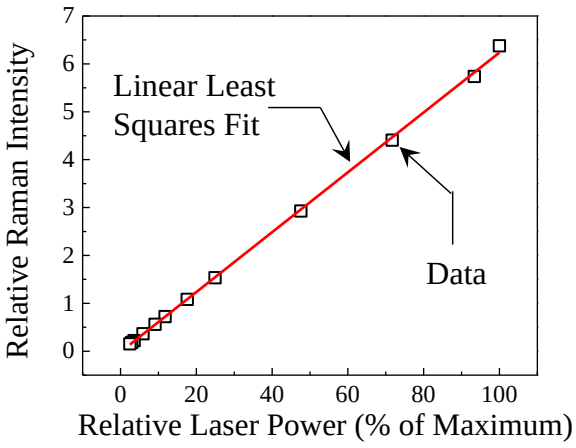

Figure S6: (a) Measurements of the relative Raman intensity ($\tilde{\nu}$ = 521 cm^{-1}) as the focus of a 632.8 nm laser beam is scanned over the cleaved edge of a Si wafer. Data are denoted by the open circles and the red curve is the best fit of the above expression for $I(x)$ to the data. The signal overshoot observed immediately to the left of the wafer edge is the result of diffraction. (b) Measurements similar to (a) but recorded at a fixed position on the Si wafer. Data were obtained as the laser power was varied up to its maximum value. The linear least-squares fit to the experimental results is shown in red and yields an R^2 value > 0.999.

7. FEM simulation of the radial and azimuthal electric field amplitudes for *d* = 2 μm microspheres

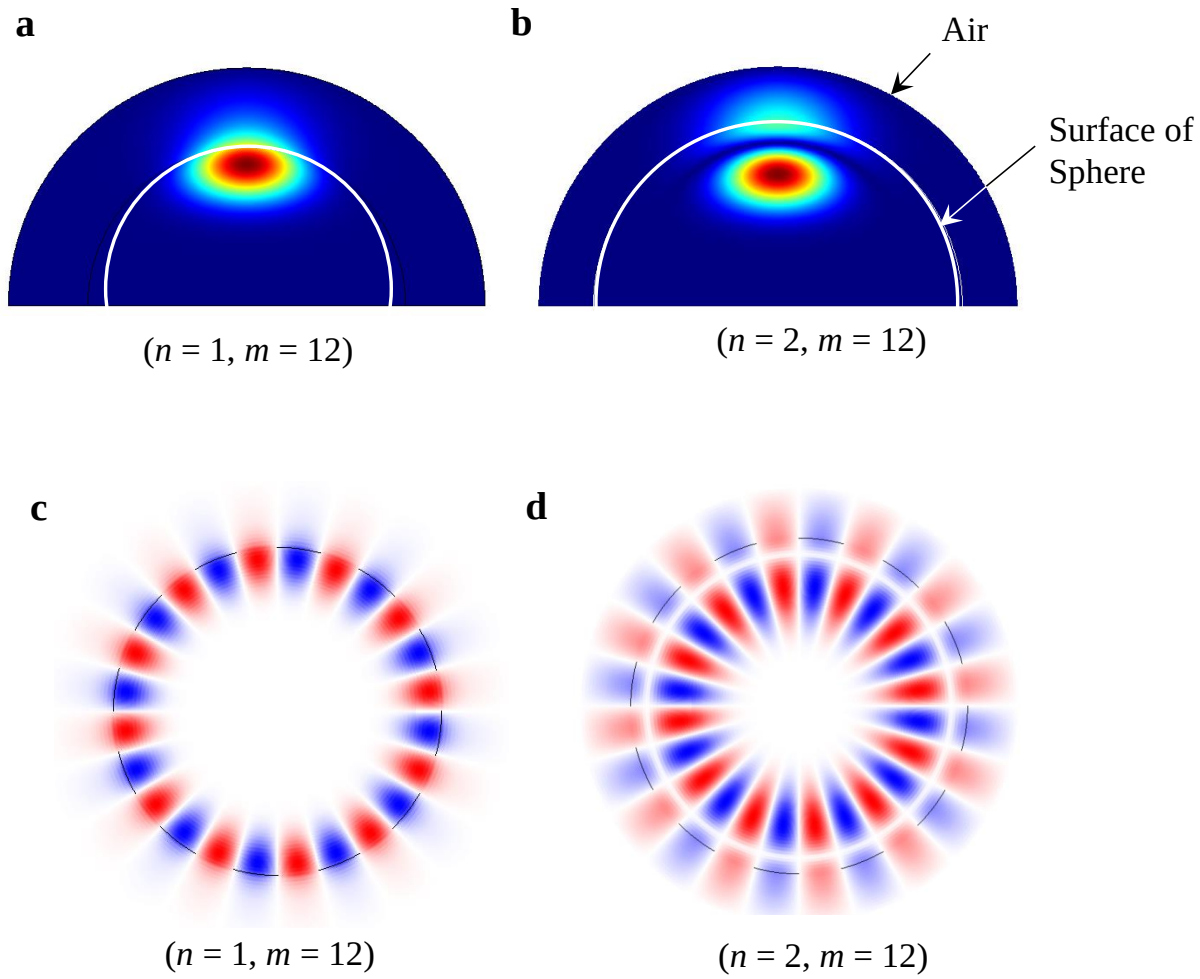

Figure S7: Calculated first and second-order radial optical eigenmodes for a d = 2 μm sphere at λ = 637.5 nm (n = 1, m = 12) and λ = 511.5 nm (n = 2, m = 12), respectively. (a, b) Color-coded maps illustrating the radial and polar variation of the square of the electric field amplitude for two modes. The white arc in both illustrations represents the surface of the polystyrene sphere. Air is assumed to lie outside the sphere. (c, d) Maps similar to those of (a) and (b) but illustrating the azimuthal dependence of the electric field amplitude. Results are given for the same modes shown in (a) and (b) but red and blue represent positive and negative values, respectively, of the field amplitude.

8. FEM simulation of radial and polar modes for d = 2 μm microspheres

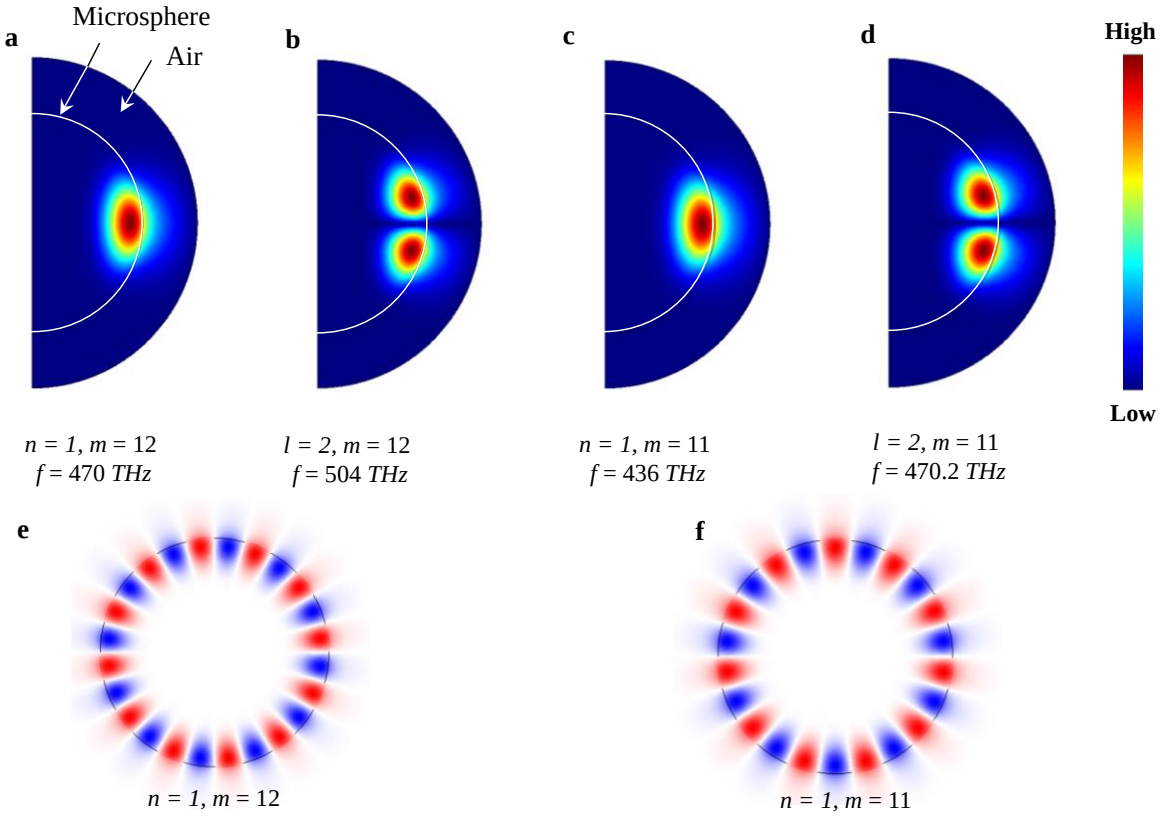

Figure S8: Calculations similar to those of Fig. S7 but for higher order polar modes of a d = 2 μm microsphere. (a - d) Color-coded maps comparing the spatial variation of $\left|\vec{E}\right|^2$ for the radial and polar modes shown, having resonant frequencies of 470.2 THz (λ = 637.5 nm), 504 THz (λ = 594.9 nm), 436 THz (λ = 686.95 nm), and 470.2 THz (λ = 637.5 nm), respectively. (e, f) Azimuthal distribution of the electric field amplitude for the n = 1, m = 11, 12 modes. Again, red and blue denote positive and negative field amplitudes, respectively.

9. FDTD simulations of electric field spatial distributions and enhanced radiative rates for optoplasmonic amplifiers with *d* = 2 μm microspheres

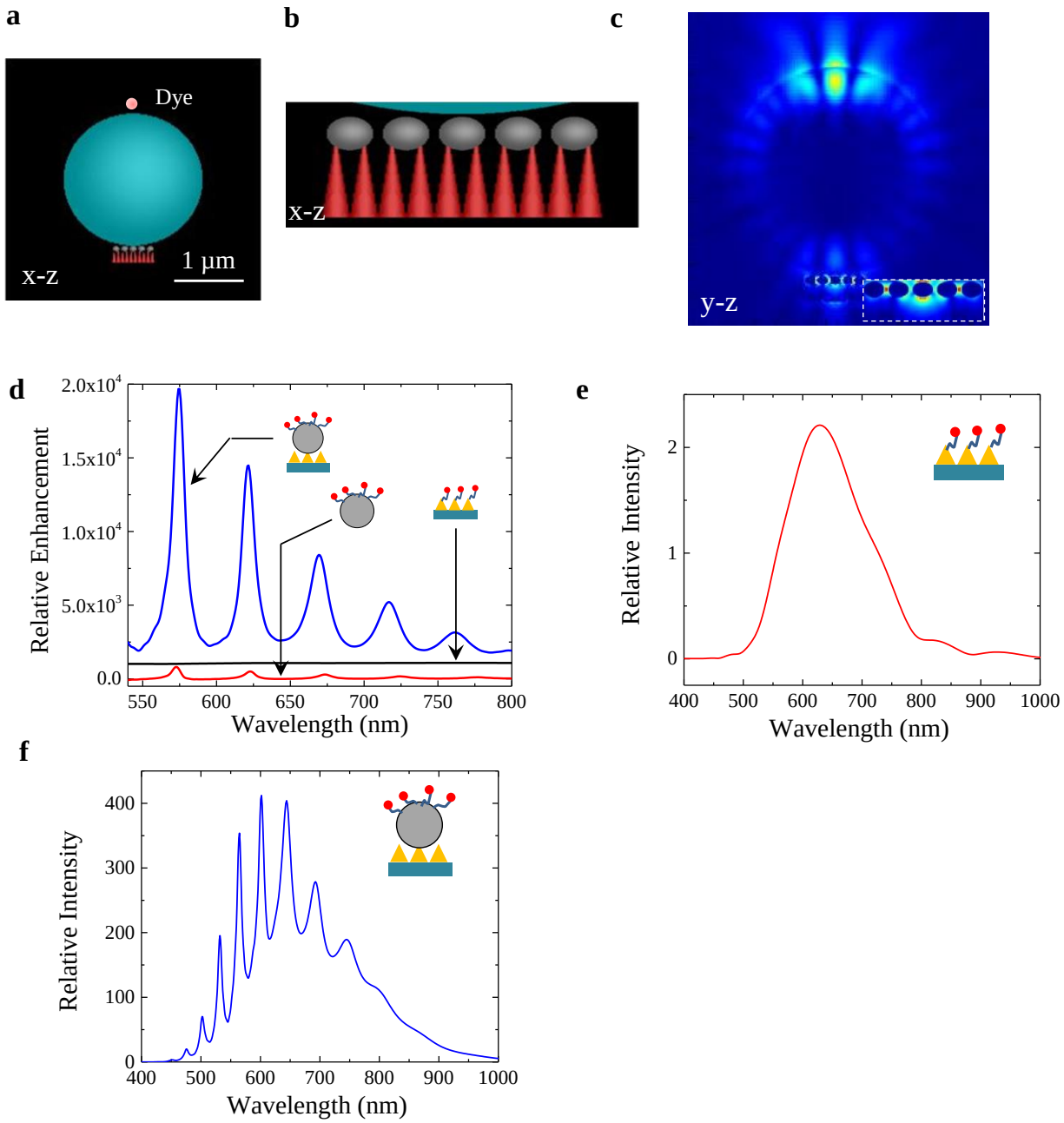

Figure S9: (a) Cross-sectional schematic diagram of the optoplasmonic amplifier, illustrating only a single dye molecule attached to a microsphere and the plasmonic substrate underneath. (b) Expanded view of the interface between the 2 μm dia. microsphere and the plasmonic substrate,

comprising Ag deposited onto nanocones. (c) Calculated electric field intensity ($|\vec{E}|^2$) in the y-z plane. Field enhancement between the Ag ellipsoids is shown by the magnified view provided by the inset. (d) Calculated enhancement in the radiative rate of the dye, defined as the power outflow of the optoplasmonic system, normalized to the power outflow from the dye itself. Results are shown for the entire optoplasmonic amplifier (in the 550 – 800 nm region), as well as for two combinations of the amplifier components. (e) Predicted emission spectrum for DyLight 650 dye tethered directly to the plasmonic substrate. The pump wavelength is assumed to be 632.8 nm. (f) Calculated emission spectrum for the full optoplasmonic amplifier in the absence of injection seeding.

10. Photoluminescence spectra of Ag-overcoated Si nanocone arrays

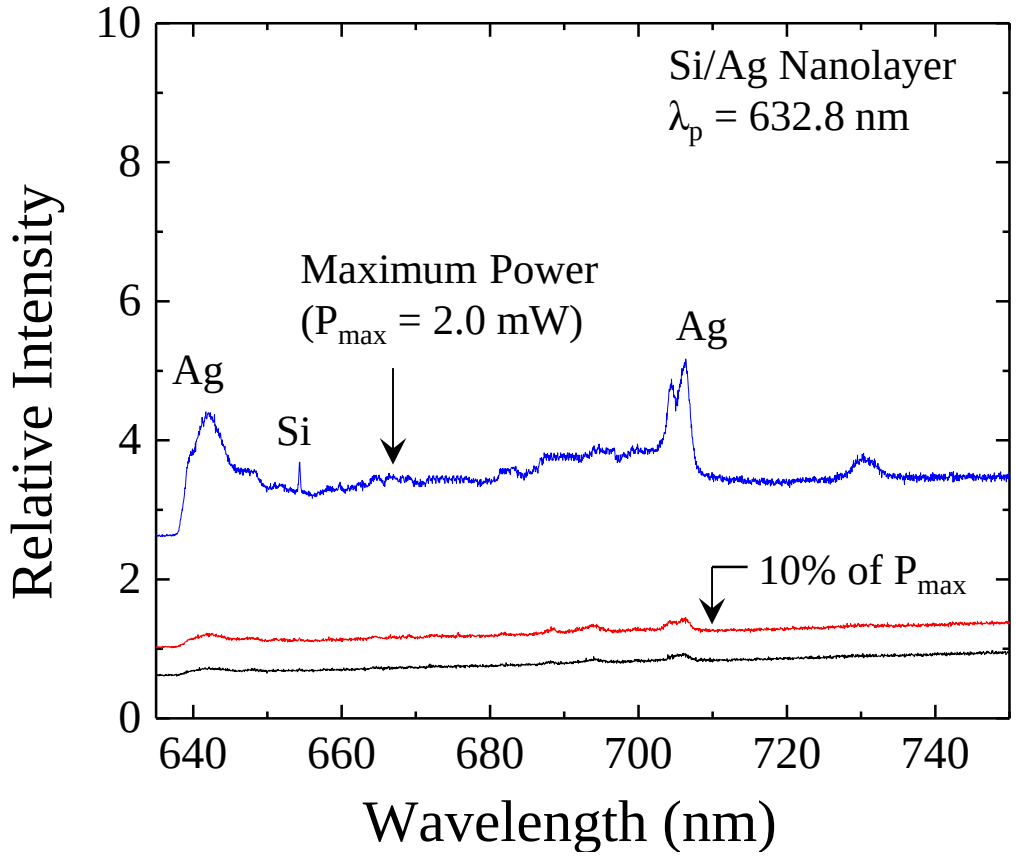

Figure S10: Photoluminescence spectra in the 635 – 750 nm region, obtained by irradiating the Si nanocone/ Ag nanolayer (~ 80 nm in thickness) structure alone. The 521 cm^{-1} Raman mode of Si is noticeable at the highest laser (λ_p = 632.8 nm) power available and the spectra presented here have been displaced vertically for clarity.

11. Impact of Ag nanolayer on the microresonator Q

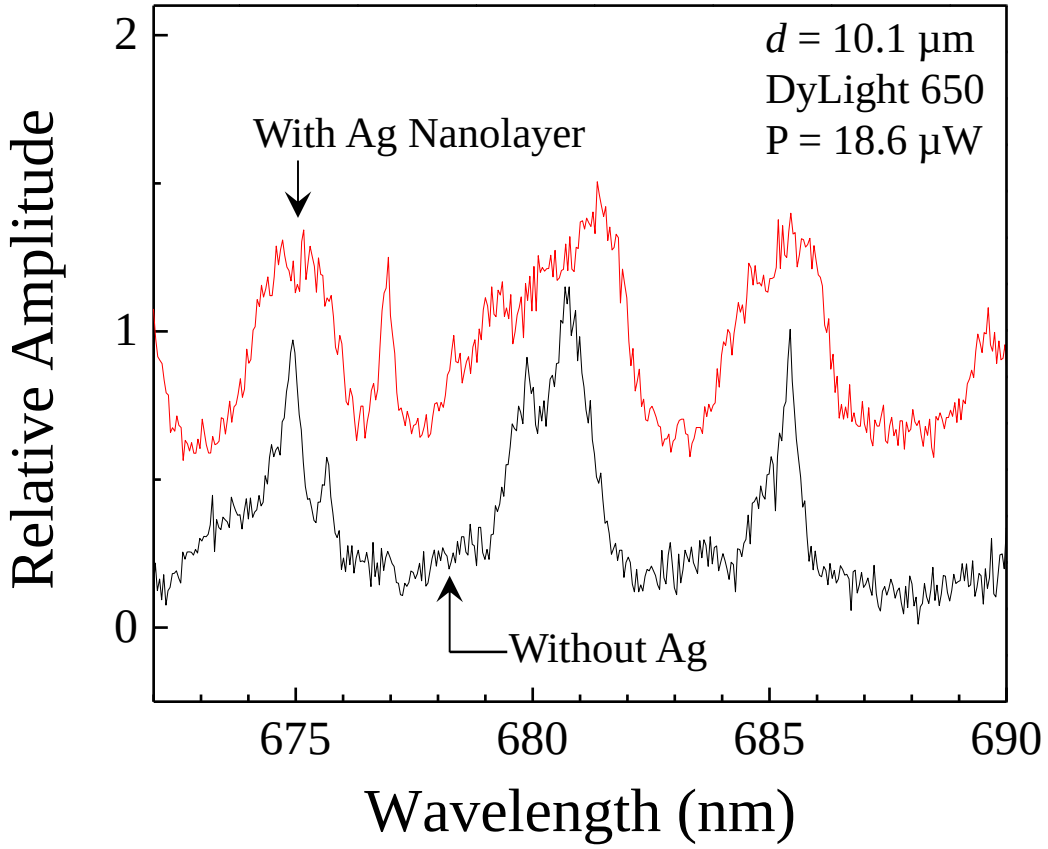

Figure S11: WGM spectra observed in the 670 – 690 nm spectral region, comparing the performance of the optoplasmonic amplifier with the Ag nanolayer in place (top trace) to the same amplifier structure except that the metal nanolayer has been removed. The two spectra have been separated vertically (and scaled separately) for clarity. In the upper spectrum, the reduction in Q, owing to the dissipative losses introduced by the metal (Ag), is evident. Calculations find that the effective Q of microresonator decreases by a factor of ~ 5 when the Si nanocone array is overcoated with Ag. Despite the drop in Q, the full amplifier (i.e., including the Ag nanolayer) generates 50% more emission over the 650 – 750 nm region than does its Ag-free counterpart.

12. Linear dependence of peak dye fluorescence intensity on dye concentration (100 nM – 1 µM)

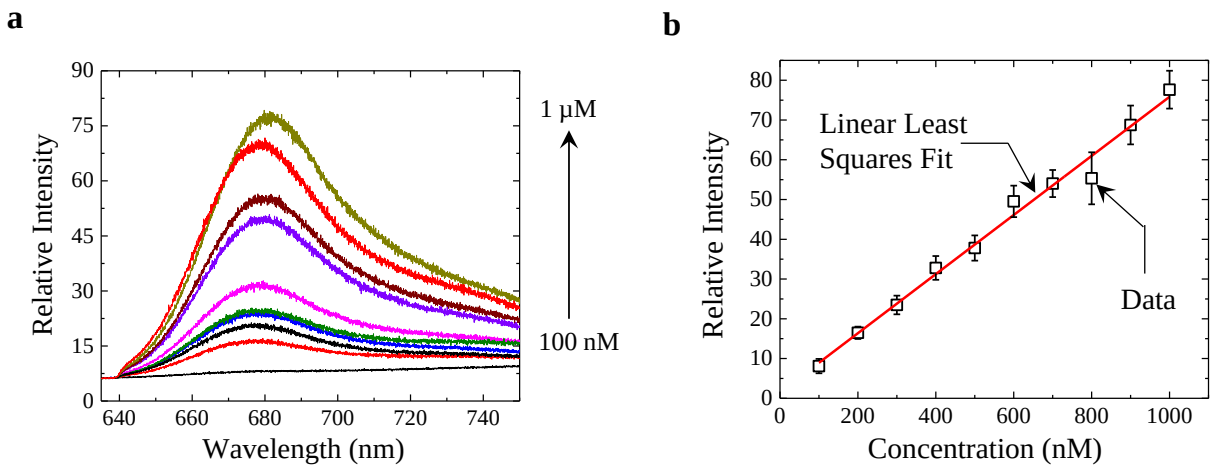

Figure S12: (a) Variation of the dye (DyLight 650) emission spectrum when the dye is conjugated with biotin-avidin and the dye concentration is increased from 100 nM to 1 µM. (b) Data illustrating the linear dependence of the peak fluorescence intensity of the dye on the concentration. Error bars denote an uncertainty of $\pm$ 1σ in the measurements.

13. Lifetime measurement for optoplasmonic system with Cy-3 dye

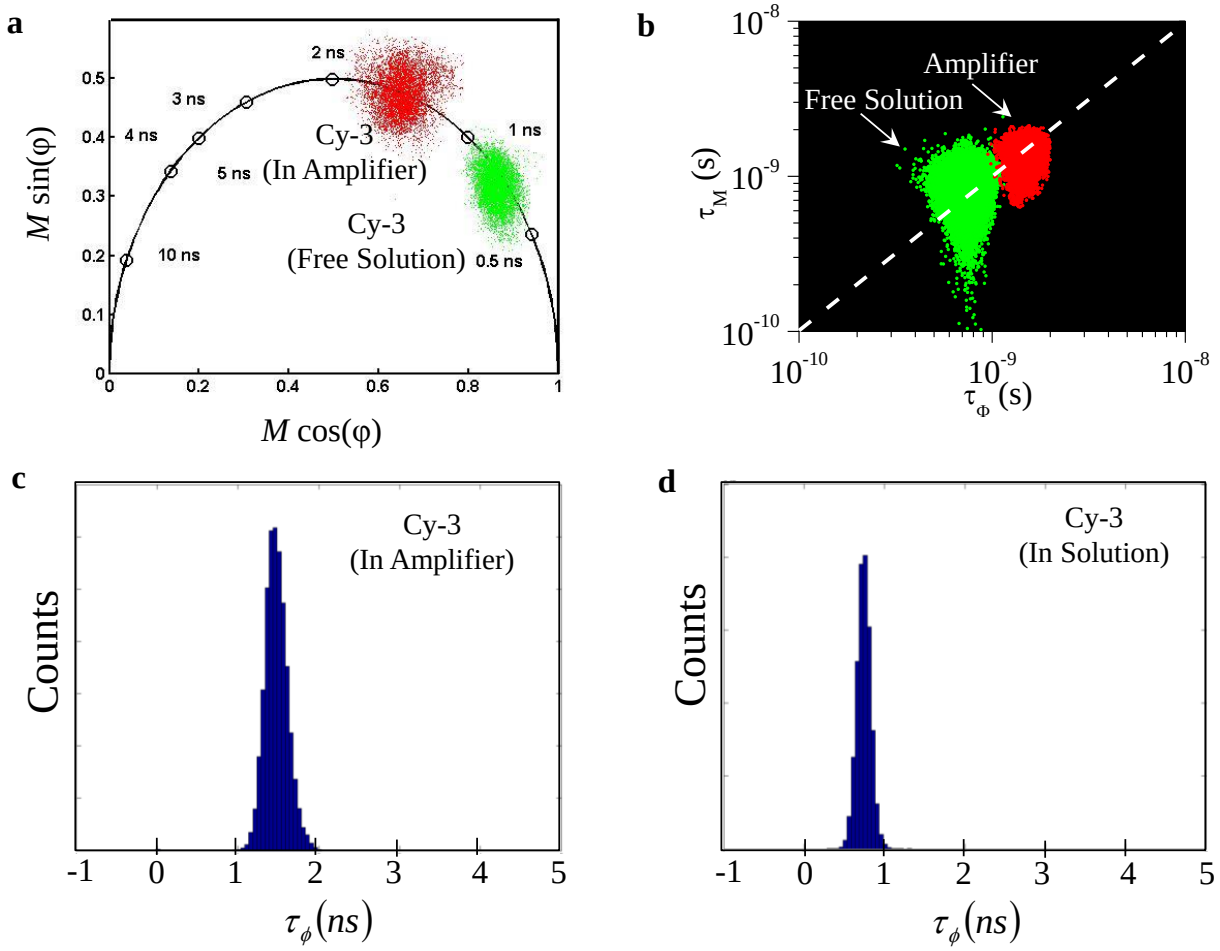

Figure S13: (a) Summary of measurements of Cy-3 lifetime by FLIM (Ref. 3). (a) Experimental polar plot representation of the Cy-3 dye fluorescence lifetime, comparing the data recorded for the dye in solution (shown in green) with those obtained for the same dye incorporated into the amplifier (red). M is the modulation ratio associated with the lifetime, ϕ is the phase, and both parameters are defined by the expression (Ref. 3): $M = \frac{1}{\sqrt{1+(\omega\tau)^2}}, \phi = \tan^{-1}(\omega\tau)$ where ω is the modulation radian frequency and τ is the radiator (dye) fluorescence lifetime. (b) Correlation between the modulation and phase lifetimes, shown as a scatter plot (conjugated with biotin-avidin) when the dye is in the amplifier or in solution (in a petridish), respectively. (c, d) Statistical distributions for the phase lifetime of Cy-3.

14. Photoluminescence spectra for an optoplasmonic structure when the dye lies at the interface between the polystyrene sphere and the plasmonic array, and not tethered to the microresonator

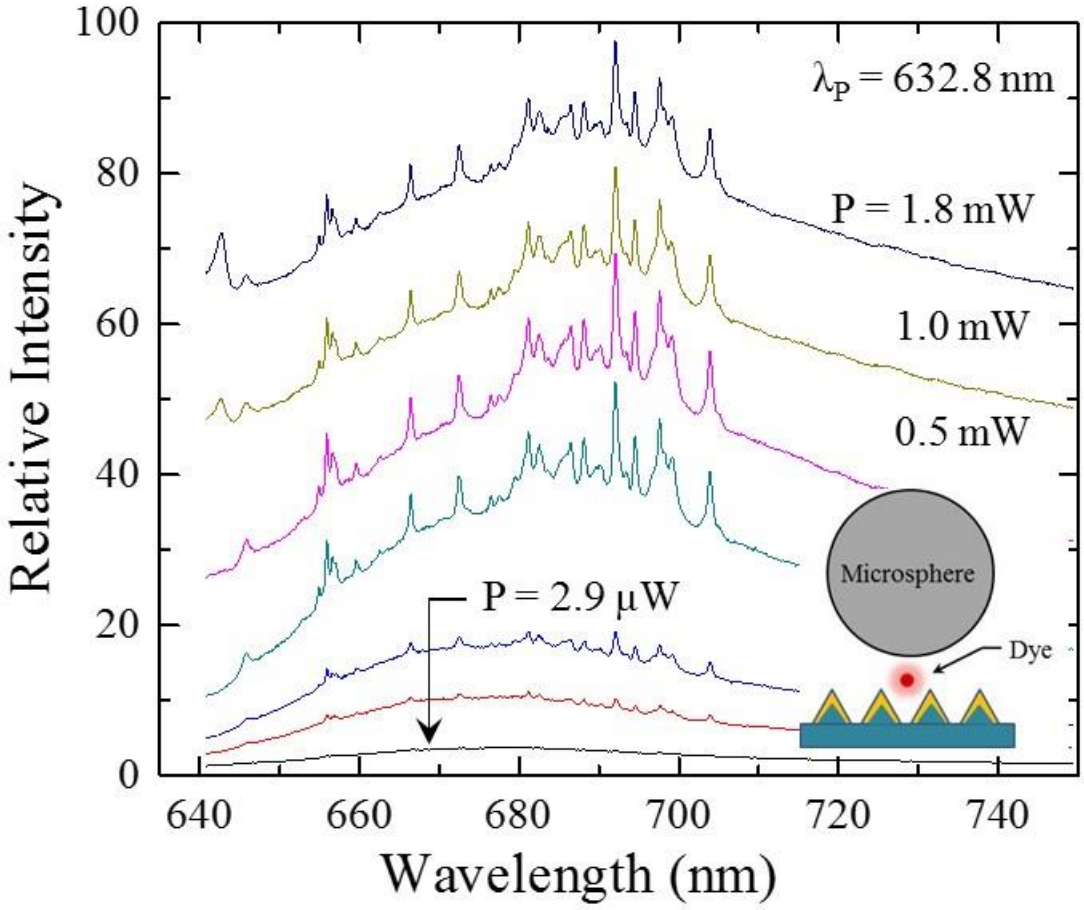

Figure S14: Photoluminescence spectra for an optoplasmonic structure similar to that of Fig. 1(a) except the dye no longer resides at the microresonator surface, but rather lies at the interface between the polystyrene sphere and the plasmonic array (as illustrated in cross-section by the inset drawing). The observed Raman features are associated with the dye (Cy-5) and the microresonator diameter (d) is 10.1 μm. These spectra were acquired with a 50x objective, an accumulation (integration) time of 10 s, and a d = 10.1 μm resonator.

15. Raman spectrum and band assignment for Cy-5 dye

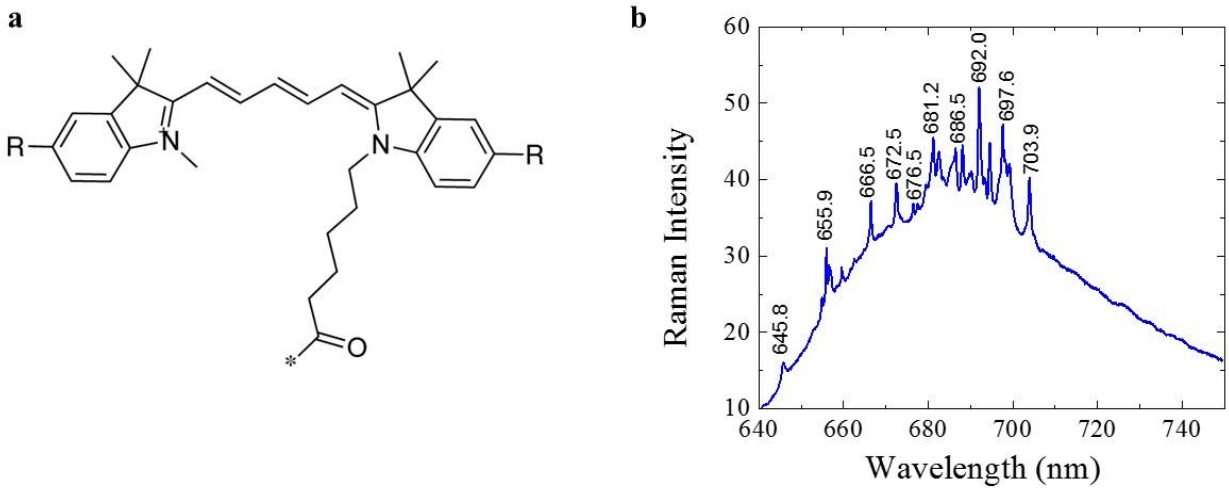

Figure S15: (a) Molecular structure of Cy-5. (b) Raman data of Cy-5 on plasmonic structure.

Table S1: Band assignments for individual features in the SERS spectra of Cy-5 in Figs. 6 and S15: The Raman modes shown in bold are responsible for the most prominent features in Figs. 6, S14 and S15.

Wavelength (nm)	Raman Shift (cm^{-1})	Assignment	References
645.8	318.8	Out of plane rocking of trimethine bridge	6
654.9	533.7	Methine bridge vibration	7
655.9	**557.5**	Methine bridge vibration	5, 7
656.6	572.4	C-C in Methine Bridge	7
659.6	641.6	In-plane bending of benzene ring	6
662.7	712.3	C-C in Methine Bridge	7
666.4	796.3	Torsion of H; Benzene ring breathing mode.	5, 8
672.4	**931.7**	C-C stretching	5, 8
676.5	1021.5	Quinoline	7
677.6	1044.6	Quinoline	7
679.5	1085.4	C-C in Methine Bridge, rocking of ethyl group	6, 7
681.2	**1122.1**	Quinoline	4, 5
682.6	1151.9	Benzene ring breathing	8
683.6	**1174.7**	Quinoline	4
685.7	1220.1	Ethyl Group	4
686.5	1235.9	Ethyl Group	4
688.1	1269.6	Ethyl Group	4, 5
689.6	1301.0	Wagging of H	8
690.2	1314.4	C-C in Methine Bridge	7
692.0	**1352.2**	Polymethine chain	4, 5
693.4	1381.0	Quinoline	4
694.6	1405.3		5
695.6	1427.3	Deformation of Benzene	8
697.6	1468.9	Quinoline	5, 6
699.1	1499.4	Rocking of ethyl group	5, 6
703.9	**1596.5**	Quinoline N-C stretching	5, 8

References

1. Y. Suzaki, A. Tachibana, Measurement of the μm sized radius of Gaussian laser beam using the scanning knife-edge, *Appl. Opt*, **14**, 2809 (1975).

2. E. C. Le Ru *et al.* SERS enhancement factors: a comprehensive study, *J. Phys. Chem. C*, **111**, 13794-13803 (2007).

3. M. R. Gartia, J. P. Eichorst, R. M. Clegg, G. L. Liu, Lifetime imaging of radiative and non-radiative fluorescence decays on nanoplasmonic surface. *Appl. Phys. Lett.* **101**, 023118 (2012).

4. J. P. Yang, R. H. Callender, The resonance Raman spectra of some Cyanine dyes. *J. Raman Spectroscopy* **16**, 319-321 (1985).

5. K. K. Maiti, A. Samanta, M. Vendrell, K. S. Soh, M. Olivo, Y.T. Chang, Multiplex cancer cell detection by SERS nanotags with cyanine and triphenylmethine Raman reporters. *Chem. Commun*. **47**, 3514–3516 (2011).

6. M. Aydin, Ö. Dede, D. L. Akins, Density functional theory and Raman spectroscopy applied to structure and vibrational mode analysis of 1,1,3,3-tetraethyl-5,5,6,6-tetrachloro-benzimidazolo carbocyanine iodide and its aggregate. *J. Chem. Phys.* **134**, 064325 (2011).

7. D. L. Akins, S. Ozcelik, H. R. Zhu, C. Guo, Aggregation-enhanced Raman scattering of a Cyanine dye in homogeneous solution. *J. Phys. Chem. A* **101**, 3251-3259 (1997).

8. D. M. Coles, A. J. H. M. Meijer, W. C. Tsoi, M. D. B. Charlton, J. S. Kim, D. G. Lidzey, A characterization of the raman modes in a j-aggregate-forming dye: a comparison between theory and experiment. *J. Phys. Chem. A* **114**, 11920–11927 (2010).